POLITECNICO
MILANO 1863

DIPARTIMENTO DI MECCANICA

mecc

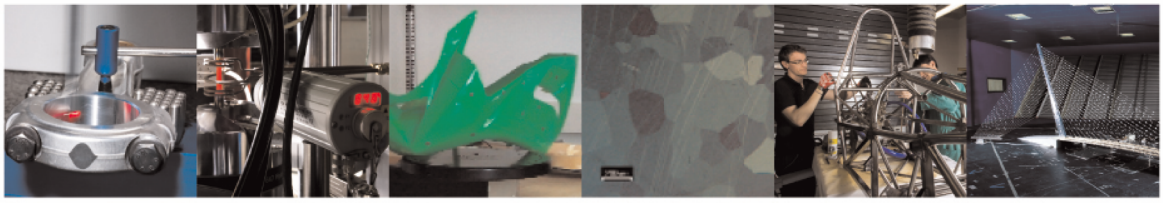

Generalisation of the linear theory of rolling contact to a single double-elliptic contact region and its application to solve non-Hertzian contact problems using extended FASTSIM

Liu B.;Bruni S.

This is an Accepted Manuscript of an article published by Taylor & Francis in Vehicle System Dynamics on 22/08/2022, available online:
https://www.tandfonline.com/doi/full/10.1080/00423114.2022.2113808

This content is provided under CC BY-NC-ND 4.0 license

Generalisation of the linear theory of rolling contact to a Single Double-Elliptic Contact Region and its application to solve non-Hertzian contact problems using extended FASTSIM

Binbin Liu, Bin Fu* and Stefano Bruni

Dipartimento di Meccanica, Politecnico di Milano, Via La Masa 1, Milano 20156, Italy.

*Corresponding author. Email: bin.fu@polimi.it

Abstract: Most contact models addressing the solution of the tangential problem, i.e. the definition of a relationship between creepages and creep forces at wheel/rail contact, assume an elliptical shape of the contact patch which is derived from the Hertz theory. In particular, the linear theory of rolling contact developed by Kalker is based on this assumption. However, it is well known that in many practical cases the shape of the contact region formed between the rail and a railway wheel can be far from elliptic. Recently, the Simple Double-Elliptic Contact (SDEC) shape has been proposed as an approximation of a wide variety of non-elliptic patches. In this paper, a formulation of the linear theory of rolling contact for a SDEC shape is proposed. The coefficients of the original linear theory for elliptic patches are maintained and four new coefficients are introduced to consider the effect of non-ellipticity. The coefficients of the theory are derived numerically using software CONTACT. Then, an extension of FASTSIM for a SDEC region is introduced and the obtained creep force curves under various conditions are compared to existing formulations of FASTSIM, using results from software CONTACT as a reference. The comparisons show that the proposed model is as fast as FASTSIM and provides more accurate solutions than existing versions of FASTSIM in terms of the resultant creep force under pure spin conditions.

Keywords: vehicle dynamics, wheel/rail contact, creepages, creep forces, linear theory, non-Hertzian, FASTSIM, wheel wear

1 Introduction

The determination through proper mathematical models of the contact forces and stresses acting between a railway wheel and the rail is crucial to setting-up models of the vehicle's running behaviour and to analyse surface and sub-surface damage phenomena taking place in wheels and rails, particularly wear and rolling contact fatigue [1][2][3]. Owing to quasi-identity [4], the contact problem is usually split in two steps solved in sequence: the normal problem and the tangential problem. The normal problem consists of determining the shape and size of the contact patch, the distribution of normal contact stresses for a prescribed normal force or normal approach of the two bodies, given the local shape of the contacting bodies. The tangential problem is concerned with determining the resulting tangential forces in the contact patch (creep forces) and, in some cases, the distribution of tangential stresses and of slip in the contact region, given the solution of the normal contact problem and the creepages defining the relative speed of the two bodies in the contact region.

Considerable progress was made in the past decades in the understanding and modelling of wheel/rail contact [5][6][7][8],which contributed to the development of the modern railway system. In this context, the Hertz theory is still widely used as it provides a simple and elegant solution in closed form, resulting in high computational efficiency and ease of use, also in combination with models of material damage [9][10][11][12]. However, it is well

known that the solution provided by the Hertzian theory may be not accurate enough in cases when the local geometry of the contacting bodies leads to a highly non-elliptic shape of the contact patch [5][7][13][14].

One well-recognized non-Hertzian (also called non-elliptic) model of wheel/rail contact is Kalker's exact theory [4], which has been implemented in software CONTACT [15]. Although the results provided by this method are highly accurate, the algorithms implementing this theory are computationally demanding and require excessive computational effort for some applications, namely multi-body systems (MBS) simulation in time domain of the running behaviour of a railway vehicle. Therefore, simplified non-Hertzian algorithms were developed to achieve a proper trade-off between accuracy and computational demand. Recent developments in this area mainly focussed on the extension to non-Hertzian condition for the normal problem, such as the Kik-Piotrowski (K-P) model [16] and its extended version EKP [17], ANALYN [18], semi-Hertzian [19] and multi-Hertzian models [20].

In contrast, most theories available to solve the tangential problem are only valid for elliptic contact patches. In particular, the linear theory of rolling contact, which assumes no slip in the contact area resulting in a linear relationship between creepages and creep force components, was defined by Kalker for elliptic contact patches. It should be noted that the linear theory has tremendous importance in railway vehicle dynamics: on one hand, it is the basis for many vehicle models, also in the context of identification, control and state estimation [21][22] and is used for stability and ride quality estimation [23]. On the other hand, the linear theory forms the basis for most simplified non-linear creep force models, particularly heuristic saturation laws and the simplified Kalker's theory implemented in algorithm FASTSIM [24].

Recently, Piotrowski et al. introduced a regularisation of non-elliptical wheel/rail contact patches in the form of a Simple Double-Elliptic Contact (SDEC) region, with the aim of computing the creep forces under non-Hertzian conditions by means of a look-up table and this algorithm is called the Kalker book of tables for non-Hertzian contact (KBTNH) [25][26]. The same regularisation can be used to extend the linear theory of rolling contact to non-Hertzian contact patches, and Vollebregt [27] first observed that this would result in the introduction of new coefficients defining the effect of spin creepage on the longitudinal creep force and the effect of longitudinal creepage on the spin moment. In this paper, the generalization proposed by Vollebregt is further extended, resulting in a new formulation that provides simple formulae to compute the creep forces according to the linear theory for any SDEC shape. The coefficients of the original linear theory for elliptic patches are maintained and four new coefficients are introduced to consider the effect of non-ellipticity. These new coefficients are obtained numerically using program CONTACT for a variety of ellipticity values, resulting in an extended version of the 'classic' table of the creepage coefficients C_{ij} from Kalker. The use of this extended theory allows to define a linear relationship between creepages and creep forces for a wide variety of non-Hertzian contact conditions, with a minimum increase of computational cost compared to the classic linear theory, provided the actual shape of the contact patch can be well approximated as a SDEC region.

Once the linear theory for the SDEC region is in place, the generalisation of saturation laws to the same non-Hertzian geometry is straightforward. Besides this, in the paper a new version of the FASTSIM method is proposed, in which one additional coefficient L_{13} is introduced to consider the effect of spin creepage on the longitudinal creep force component.

A modified expression is also proposed for the other flexibility coefficients, L_{11}, L_{22} and L_{23}, to make the results of FASTSIM for the non-slip condition consistent with the linear theory for the SDEC region. This new formulation of FASTSIM can improve the accuracy of the method when applied to non-Hertzian contact patches that are passible of being regularised in the form of a SDEC region, solving the issues related to the definition of the flexibility parameters in non-Hertzian conditions [16][25][28][29].

The paper is organised as follows. Section 2 recalls the geometric features of the SDEC region. Section 3 extends the linear theory to the SDEC contact conditions and determines the new extended table of the coefficients of the linear theory for Poisson's ratio $\upsilon = 0.25$. Section 4 introduces the modified FASTSIM algorithm for the SDEC region (FASTSIM-SDEC). Section 5 compares the results of FASTSIM-SDEC to two other FASTSIM formulations, using CONTACT as a term of reference. Finally, concluding remarks are provided in the last section.

2 Geometry of the SDEC region

The geometry of a generic SDEC region is shown in Figure 1: the length of the contact patch along the rolling direction x is $2a$, the width is $2b$, and the origin O of the contact patch is located at the initial point of contact (also known as the geometrical point of contact) of the contacting bodies, which is shifted by y_0 in lateral direction with respect to the mid-point of the segment connecting the two extremities of the contact patch in lateral direction. The SDEC shape was selected in the KBTNH algorithm to regularize the non-elliptic contact regions. The reasons for this choice are, on one hand, that this shape has a simple analytical expression while featuring quasi-Hertzian properties [16] and, on the other hand, that SDEC-like shapes of the contact patch are frequently found and even observed experimentally for typical wheel and rail profiles [25][30][31].

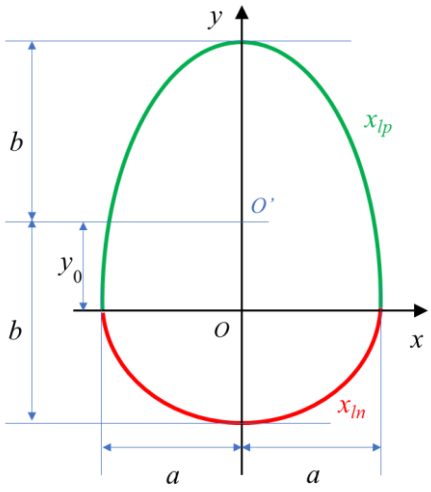

Figure 1 The SDEC patch: *x*-rolling direction, *y*-lateral direction

The SDEC region is described by the following equation:

$$\begin{cases} \frac{x^2}{a^2} + \frac{y^2}{b^2(1+\psi)^2} = 1 & (y > 0) \\ \frac{x^2}{a^2} + \frac{y^2}{b^2(1-\psi)^2} = 1 & (y \leq 0) \end{cases} \quad (1)$$

where parameter ψ, called the shape number, is an indicator for the deviation of the contact patch shape from an ellipse and is defined as follows:

$$\psi = y_0/b \tag{2}$$

It is observed from Eq. (2) that the shape number takes values between -1 and 1, with ψ =0 representing the case of an elliptic contact patch. The leading edge $x_l(y)$ of the SDEC patch is defined by two branches of ellipse, having different expression for positive and negative values of coordinate *y*:

$$\begin{cases} x_{lp}(y) & = a\sqrt{1-\frac{y^2}{b^2(1+\psi)^2}} \quad (y>0) \\ x_{ln}(y) & = a\sqrt{1-\frac{y^2}{b^2(1-\psi)^2}} \quad (y\le 0) \end{cases} \tag{3}$$

Compared to the elliptic patch, the SDEC contact region has only one additional parameter, i.e. the shape number ψ.

One interesting property of the SDEC region is that, if a semi-elliptic normal pressure distribution is assumed for the SDEC patch in the rolling direction as follows:

$$p_n(x,y) = \frac{p_0}{a}\sqrt{x_l^2(y)-x^2} \tag{4}$$

the relationship between normal load *N* and the maximum pressure p_0 is $N = \frac{2}{3}p_0\pi ab$ as for a Hertzian contact [25]. The solution of the tangential contact problem for a SDEC region is now implemented in the CONTACT program [15], assuming the distribution of normal pressure according to Eq. (4) but in this implementation (referred hereafter as CONTACT-SDEC) the origin of the *x-y* reference is located at the mid-point of the contact region in lateral direction, point *O'* in Figure 1, instead than at the initial contact point.

3 The linear theory for the SDEC region

The linear theory for creepage-creep force relationship assumes the traction bound to be infinite, so that adhesion of the two bodies in rolling contact takes place over the entire contact patch. The solution of this problem was provided by Kalker for an elliptic contact patch [4] and is extended here to the SDEC region.

To this aim, we first recall the expression of the rigid slip vector **w**, i.e. the difference in the tangential velocity of the two contacting surfaces produced by the rigid motion of the bodies, normalised by the rolling velocity *V*, as a function of the longitudinal and lateral creepage components ν_x and ν_y and of the spin creepage ϕ:

$$\mathbf{w} = \begin{bmatrix} \nu_x - \phi y \\ \nu_y + \phi x \end{bmatrix} \tag{5}$$

In Eq.(5) *x* and *y* are the coordinates of a generic point in the contact patch with respect to the reference introduced in Figure 1: it follows that the creepage components in Eq.(5) are defined with respect to the initial contact point.

The true slip **s** is the velocity of a particle of the wheel with respect to the contacting particle of the rail normalised by the rolling velocity *V*. It is expressed as the sum of the rigid slip given by Eq. (5) and the deformation slip due to local elastic displacements of the two bodies described by vector **u** [4]:

$$\begin{aligned} \mathbf{s} &= \mathbf{w} + \frac{1}{V}\dot{\mathbf{u}} \\ &= \begin{bmatrix} \nu_x - \phi y \\ \nu_y + \phi x \end{bmatrix} - \frac{\partial \mathbf{u}}{\partial x} + \frac{1}{V}\frac{\partial \mathbf{u}}{\partial t} \end{aligned} \tag{6}$$

Kalker's linear theory was derived under steady-state conditions ($\frac{\partial \mathbf{u}}{\partial t} = \mathbf{0}$) for the Hertzian elliptic contact when the true slip approaches zero (**s** = 0). Here, we take the same assumption for the SDEC patch, so that Eq. (6) becomes:

$$\frac{\partial \mathbf{u}}{\partial x} = \begin{bmatrix} \nu_x - \phi y \\ \nu_y + \phi x \end{bmatrix} \tag{7}$$

Using the traction-displacement relationship based on the general elasticity theory and integrating the traction over the contact area, the linear relation between the creepages and the creep forces are obtained as follows for a non-elliptic contact area.

$$\left.\begin{aligned} F_x &= -Gc^2 C_{11}^s \nu_x - Gc^2 C_{12}^s \nu_y - Gc^3 C_{13}^s \phi \\ F_y &= -Gc^2 C_{21}^s \nu_x - Gc^2 C_{22}^s \nu_y - Gc^3 C_{23}^s \phi \end{aligned}\right\} \tag{8}$$

where G is the combined shear modulus, $c = \sqrt{ab}$ and C_{11}^s, C_{12}^s, C_{13}^s, C_{21}^s, C_{22}^s and C_{23}^s are the coefficients of the linear theory for the SDEC patch, replacing the C_{11}, C_{22} and C_{23} coefficients considered in Kalker's linear theory. Coefficient C_{13}^s defining the effect of spin creepage on the longitudinal creep force was introduced by Alonso and Gimenez in [28] for a generic non-Hertzian contact patch and by Vollebregt [27] for a SDEC contact region. In this paper we propose a parametrization of the coefficients in Eq. (8) as a function of the shape number ψ, resulting in a general expression of the linear creep forces for any SDEC region. Vollebregt [27] also introduced a companion term C_{31}^s defining the effect of longitudinal creepage on the spin moment M_z. In this paper the expression of the spin moment according to the generalized linear theory is not addressed, considering that the effect of the spin moment on vehicle dynamics is generally negligible.

It is shown below that the two coefficients C_{12}^s and C_{21}^s are zero or take very small values for all SDEC shapes and can be neglected. However, the C_{13}^s coefficient takes non-negligible values and needs to be considered. This coefficient has no counterpart in Kalker's linear theory for elliptic contacts and arises from the fact that the SDEC shape is not symmetric with respect to the *x*-axis.

3.1 Determination of the linear theory coefficients for the SDEC region

The linear theory coefficients of introduced in Eq. (8) can be obtained from integrals performed over the SDEC contact region of the Boussinesq-Cerruti expressions [32] defining the in-plane displacement of a point belonging to the surface of an elastic half-space, subject to a tangential traction applied at some point in the same surface. This approach was implemented in MATLAB, using a discretisation of the SDEC region in rectangular cells and a zero-order approximation of the tangential tractions along the *x* and

y directions. However, this method was found to be sensitive to the minimum size of the cells along the *x* direction and tended to become progressively inaccurate for very small values of the ellipticity parameter *g*. For this reason, the coefficients were instead determined from the incremental ratios of the creep force components F_x and F_y obtained from CONTACT-SDEC when small non-zero values of the three creepage components are applied:

$$\left.\begin{aligned} C_{11}^{s} &= -\frac{\Delta F_{xx}}{\Delta \nu_x}\cdot\frac{1}{Gc^2}\ ; \quad C_{12}^{s} = -\frac{\Delta F_{xy}}{\Delta \nu_y}\cdot\frac{1}{Gc^2}\ ; \quad C_{13}^{s} = -\frac{\Delta F_{x\phi}}{\Delta \phi}\cdot\frac{1}{Gc^3} \\ C_{21}^{s} &= -\frac{\Delta F_{yx}}{\Delta \nu_x}\cdot\frac{1}{Gc^2}\ ; \quad C_{22}^{s} = -\frac{\Delta F_{yy}}{\Delta \nu_y}\cdot\frac{1}{Gc^2}\ ; \quad C_{23}^{s} = -\frac{\Delta F_{y\phi}}{\Delta \phi}\cdot\frac{1}{Gc^3} \end{aligned}\right\} \tag{9}$$

where $\Delta\nu_x$, $\Delta\nu_y$ and $\Delta\phi$ are small values of longitudinal, lateral and spin creepage, ΔF_{xx}, ΔF_{xy} and $\Delta F_{x\phi}$ are the longitudinal creep forces produced by the application of $\Delta\nu_x$, $\Delta\nu_y$ and $\Delta\phi$ respectively and ΔF_{yx}, ΔF_{yy}, $\Delta F_{y\phi}$ are the lateral creep forces produced by the application of the same three creepage components.

It is recalled from Section 2 that in CONTACT-SDEC the origin of the *x*-*y* reference is located at point *O*' instead than at the initial contact point *O* (see Figure 1) which is the origin of the contact patch considered in this study. Therefore, the calculation of the creep forces using CONTACT-SDEC was performed considering a modified value ν_x' of the longitudinal creepage as follows:

$$\nu_x' = \nu_x - \phi y_0 \tag{10}$$

In this way, the values of the coefficients obtained from Eq. (9) are consistent with the reference choice adopted in this paper.

In this study, the coefficients of the linear theory for the SDEC region are computed for different ellipticity values in the range $0.1 \div 10$, for different shape numbers in the range $-0.8 \div 0.8$ and for a single value of Poisson's ratio equal to 0.25. It was found that the numerical approximation of the coefficients from Eq. (9) was sensitive to the ellipticity of the contact. Therefore, in order to guarantee the accuracy of the calculation, the size of the cells in the grid discretising the contact region in program CONTACT and the values of the creepage components $\Delta\nu_x$, $\Delta\nu_y$ and $\Delta\phi$ were tuned separately for different groups of values of ellipticity *g* until obtaining that for elliptic contact regions ($\psi = 0$) the procedure provides the values C_{11}, C_{22} and C_{23} well below 1% of error compared to those listed in the original table from Kalker [4]. The maximum and average error of the C_{11}, C_{22} and C_{23} coefficients compared to Kalker's values obtained for the shape number $\psi = 0$ and for all ellipticity values are 0.85% and 0.26% respectively.

The coefficients obtained for a family of SDEC patches having ellipticity $g = 0.5$ are shown as function of the shape number ψ in Figure 2, as an example of the results found. The coefficients obtained for other ellipticity values show similar trends with the shape number ψ and are not shown for the sake of brevity.

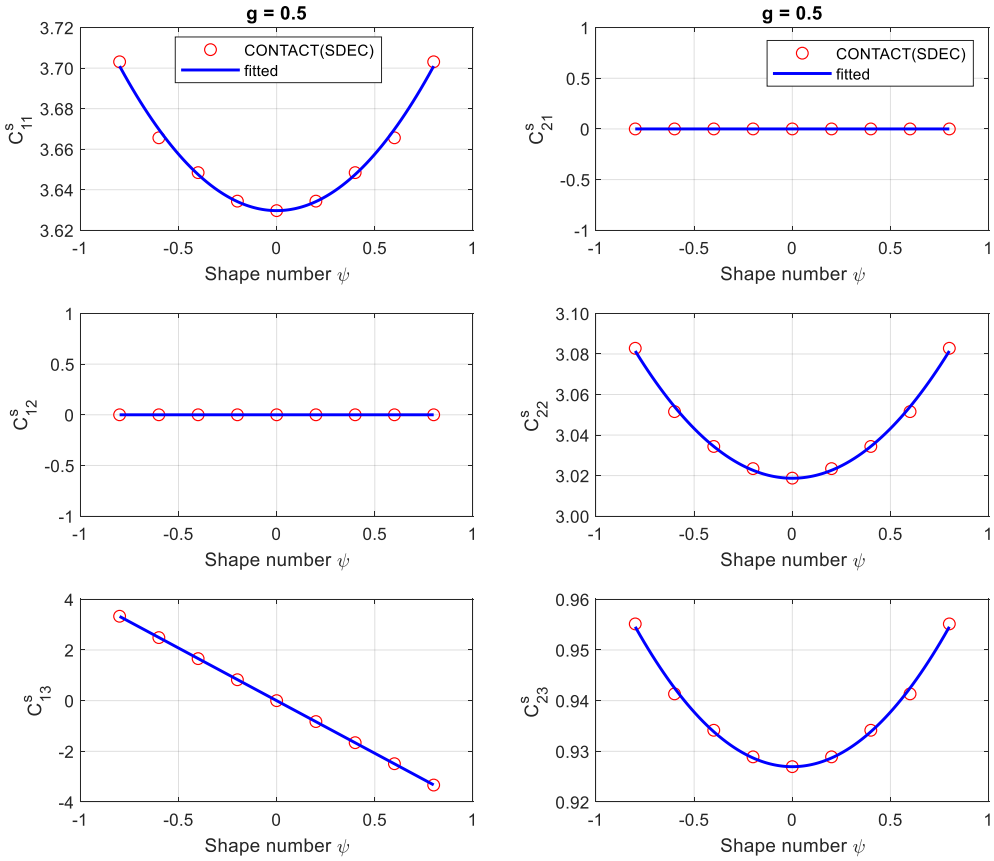

Figure 2 Coefficients of the linear theory of rolling contact for the SDEC region as a function of the shape number for g = 0.5

First of all, it is noted that coefficients C^s_{12} and C^s_{21} take negligible values (three orders of magnitude lower than the other coefficients) for all shape numbers: this circumstance is not specific of the case shown in Figure 2, and instead applies to any combination of shape number and ellipticity considered in this study. This happens because, under the assumption of infinite traction bound, the following situation arises:

i) tractions in y direction produced by a longitudinal creepage ν_x and the tractions in x direction produced by a transversal creepage component ν_y are both small in most of the contact patch, becoming non-negligible only close to the trailing edge of the contact patch;

ii) the contributions from cells located close to the trailing edge of the patch are opposite in sign for cells located at opposite sides of the initial contact point (red and green branches of the trailing edge in Figure 1) and tend to cancel with each other.

Therefore, it is concluded that the contribution of lateral creepage ν_y to the longitudinal force F_x and the contribution of the longitudinal creepage ν_x to the lateral force F_y are both negligible for SDEC contact region, and Eq. (8) can be simplified to:

$$\left.\begin{aligned} F_x &= -Gc^2 C^s_{11}\nu_x - Gc^3 C^s_{13}\phi \\ F_y &= -Gc^2 C^s_{22}\nu_y - Gc^3 C^s_{23}\phi \end{aligned}\right\} \tag{11}$$

Next, we see in Figure 2 that coefficients C_{11}^s, C_{22}^s and C_{23}^s show an even trend with the shape number, which are well approximated by a quadratic function of the shape number ψ, shown by a blue solid line in the figure. On the other hand, the C_{13}^s coefficient is an odd function of the shape number, which is consistent with the distribution of the longitudinal stresses in the SDEC patch, see Figure 4 from reference [25] for a qualitative visualisation based on the simplified theory. Finally, it is noted that the trend of the C_{13}^s coefficient with the shape number is well approximated by a linear function, shown in Figure 2 by a blue solid line.

Based on the above observations, we propose the following equation to estimate the coefficients of the linear theory for the SDEC contact patch appearing in Eq. (11):

$$\left.\begin{aligned} C_{11}^s &= C_{11} + B_{11}\psi^2 \\ C_{13}^s &= -K_{13}\psi \\ C_{22}^s &= C_{22} + B_{22}\psi^2 \\ C_{23}^s &= C_{23} + B_{23}\psi^2 \end{aligned}\right\} \tag{12}$$

where C_{11}, C_{22} and C_{23} are the coefficients of the linear theory for the elliptic contact patch (i.e. the ones available from the classic Kalker's table), B_{11}, B_{22} and B_{23} are the coefficients of the second-order term in the expression of C_{11}^s, C_{22}^s and C_{23}^s as functions of the shape number and K_{13} is the coefficient describing the linear trend of C_{13}^s with the shape number.

Eq. (11) and Eq. (12) altogether provide the generalisation of Kalker's linear theory to the SDEC region. Of course, for the shape number $\psi = 0$ the usual linear theory for elliptic patches is obtained. It should be noted that this approach is not restricted to a shape of the contact patch exactly matching the SDEC geometry, as many non-elliptic contact patches can be approximated to a satisfactory degree of approximation as a SDEC region by applying the following criteria [25][26]:

i) the contact area of the equivalent SDEC region is equal to the actual contact area A_n, i.e. $\pi ab = A_n$, where a and b are the semi-axes of the SDEC region.
ii) the semi-axes ratio of the SDEC is equal to the ratio of the actual contact length L_n to width W_n, i.e. $a/b = L_n/W_n$.
iii) the origin of the SDEC patch is located at the initial point of contact which is defined as the point where the two bodies touch each other without transmitting load.

The regularization is schematically shown in Figure 3 where the area of the contact patch is A_n with length L_n and width W_n. The distances from the lateral extremities of the patch to the geometrical point of contact W_1 and W_2 define the parameter y_0^*:

$$y_0^* = (W_1 - W_2)/2 \tag{13}$$

Therefore, the equivalent SDEC is determined with the following parameters:

$$\left.\begin{aligned} a &= \sqrt{\frac{A_n L_n}{\pi W_n}} \\ b &= \sqrt{\frac{A_n W_n}{\pi L_n}} \\ \psi &= \frac{2y_0^*}{W_n} = \frac{W_1 - W_2}{W_n} \end{aligned}\right\} \tag{14}$$

More details on the regularization can be found in [25]. It should be noted that typical wheel/rail profile combinations often produce SDEC-like contact regions [25][30][31], the highly non-elliptic contact region unlike SDEC depicted in Figure 3 is used for highlighting the differences between the actual contact and equivalent SDEC region for demonstration.

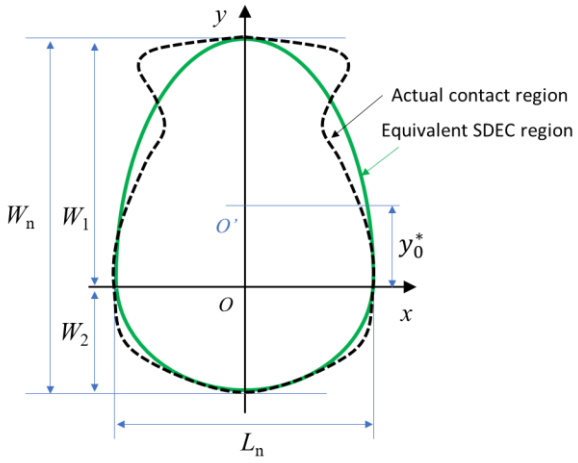

Figure 3 Regularization of a general non-elliptic contact region by a SDEC region

The generalisation of the linear theory to SDEC contact patches requires that four additional coefficients are obtained. Like for the coefficients of Kalker's linear theory, these can be pre-computed and listed in a table as functions of the ellipticity g and of Poisson's ratio. This means the additional computational effort required to apply the linear theory for a SDEC region instead of an elliptic patch is very limited, as it amounts to the interpolation of four additional parameters from the table and the computing the values of the coefficients for the SDEC region according to Eq. (12).

Table 1 provides the values of the coefficients of the linear theory for the SDEC region for different ellipticity values and for a single value of Poisson's ratio υ = 0.25. To maintain consistency with the classic table published by Kalker, the values for coefficients C_{11}, C_{22} and C_{23} are set to the same values as in Kalker's table, and not to the values obtained from CONTACT-SDEC. It should be recalled that the values of these coefficients were originally found by Kalker using a polynomial approximation of the elastic displacements in the contact patch, which involves an approximation presumably comparable to the differences found between the 'classic' values from Kalker and the ones obtained using CONTACT-SDEC.

Finally, it is worth pointing out that the difference between the C_{11}, C_{22} and C_{23} coefficients and their counterparts for a SDEC region C_{11}^s, C_{22}^s and C_{23}^s is quite small for any value of the ellipticity g and shape number ψ and can probably be considered negligible for practical purposes. However, the value of the C_{13}^s coefficient is definitely non-negligible unless the shape factor is close to zero, and this term involves an important difference in the creep forces obtained for the same creepages depending on whether the contact patch shape is approximated to an elliptic or SDEC region.

Table 1 Coefficients of the linear theory of rolling contact for a SDEC region for Poisson's ratio υ = 0.25.

g	C_{11}	C_{22}	C_{23}	K_{13}	B_{11}	B_{22}	B_{23}
0.1	3.31	2.52	0.473	8.88	0.029	0.037	0.006
0.2	3.37	2.63	0.603	6.33	0.056	0.065	0.019
0.3	3.44	2.75	0.715	5.23	0.080	0.082	0.030
0.4	3.53	2.88	0.823	4.59	0.097	0.093	0.038
0.5	3.62	3.01	0.929	4.16	0.115	0.100	0.044
0.6	3.72	3.14	1.03	3.86	0.121	0.103	0.048
0.7	3.81	3.28	1.14	3.63	0.123	0.102	0.051
0.8	3.91	3.41	1.25	3.45	0.119	0.097	0.051
0.9	4.01	3.54	1.36	3.30	0.123	0.096	0.055
1.0	4.12	3.67	1.47	3.18	0.143	0.109	0.063
1/0.9	4.22	3.81	1.59	3.07	0.139	0.104	0.064
1/0.8	4.36	3.99	1.75	2.95	0.132	0.098	0.063
1/0.7	4.54	4.21	1.95	2.84	0.145	0.105	0.071
1/0.6	4.78	4.50	2.23	2.73	0.131	0.089	0.065
1/0.5	5.10	4.90	2.62	2.60	0.134	0.091	0.066
1/0.4	5.57	5.48	3.24	2.51	0.123	0.077	0.070
1/0.3	6.34	6.40	4.32	2.38	0.121	0.075	0.072
1/0.2	7.78	8.14	6.63	2.29	0.107	0.064	0.080
1/0.1	11.7	12.8	14.6	2.30	0.080	0.050	0.088

4 The FASTSIM algorithm for the SDEC region

Based on the generalisation of the linear theory presented in the previous section, any non-linear creep force model which makes use of the linear theory can also be extended to deal with a non-elliptic contact patch regularised as a SDEC region replacing Kalker's expression of the linear creepage-creep force relation with those found for a SDEC patch. For instance, the generalisation of Shen-Hedrick-Elkins formulae [33] for a SDEC region is straightforward: the unsaturated creep forces are computed using Eq. (11) and Eq. (12) in place of the classic formulation of the linear theory and then the same heuristic saturation law is applied.

Another contact model based on the linear theory is the simplified contact theory implemented by the FASTSIM algorithm, in which the linear theory is used to determine the flexibility parameters then used to determine the distribution of tangential stresses and the resulting creep forces. In this section, a new formulation of FASTSIM for the SDEC region is presented, introducing a new flexibility parameter L_{13} to consider the effect of spin on the longitudinal component of the creep force. In this new formulation of FASTSIM, the unsaturated distribution of tangential stresses in the rolling direction x and in lateral direction y are defined as follows:

$$\left.\begin{aligned} p_x(x,y) &= \left(\frac{1}{L_{11}}\nu_x - \frac{1}{L_{13}}\phi y\right)(x - x_l) \\ p_y(x,y) &= \frac{1}{L_{22}}\nu_y(x - x_l) + \frac{1}{2L_{23}}\phi(x^2 - x_l^2) \end{aligned}\right\} \tag{15}$$

with L_{11}, L_{22} and L_{23} the flexibility parameters considered by the standard FASTSIM method and L_{13} the new flexibility parameter.

The unsaturated creep forces are obtained by analytical integration of the stress over the contact area as follows:

$$\left.\begin{aligned} F_x &= \int_{-b+y_0}^{b+y_0}\int_{-x_l}^{x_l} p_x dxdy = -\frac{8ac^2\nu_x}{3L_{11}} + \frac{2c^4\phi\psi}{L_{13}} \\ F_y &= \int_{-b+y_0}^{b+y_0}\int_{-x_l}^{x_l} p_y dxdy = -\frac{8c^2a\nu_y}{3L_{22}} - \frac{\pi a^2c^2\phi}{4L_{23}} \end{aligned}\right\} \tag{16}$$

It is seen from Eq. (16) that the contribution of the spin creepage to the longitudinal creep force is also a function of the shape number, which can increase or decrease the total force depending on the sign of the shape number.

By equating the expressions of the unsaturated creep forces from Eq. (16) to those defined by the linear theory generalised to a SDEC region, Eq. (11), the flexibility parameters are determined as follows:

$$\left.\begin{aligned} L_{11} &= \frac{8a}{3GC_{11}^s} \\ L_{13} &= \frac{2c}{GK_{13}} \\ L_{22} &= \frac{8a}{3GC_{22}^s} \\ L_{23} &= \frac{\pi a^2}{4GcC_{23}^s} \end{aligned}\right\} \tag{17}$$

In Eq. (17) the flexibility parameters L_{11}, L_{22} and L_{23} maintain their usual expression like in the standard formulation of FASTSIM, but the C_{11}, C_{22} and C_{23} coefficients of Kalker's linear theory are replaced by the new coefficients C_{11}^s, C_{22}^s and C_{23}^s. Therefore, the values of these coefficients are changing with the shape number, despite this effect is small. The new flexibility parameter L_{13} is defined based on the new parameter K_{13} of the linear theory modified for the SDEC geometry.

Once the flexibility parameters are determined, the unsaturated stress distributions are computed according to Eq. (15), and the saturation is checked at each cell of the discretised contact patch by comparing the resultant stress to the traction bound. Two formulations for the traction bound are often implemented in the FASTSIM algorithm, namely a semi-elliptic defined as the Hertzian normal pressure multiplied by the friction coefficient and a parabolic expression from the simplified theory. The motivations and consequences of the application of the different traction bounds in FASTSIM have been discussed in past works [12][34][35]. In the following calculations, a parabolic traction bound is assumed according to the expression below to improve the creep force evaluation.

$$\tau_{max}(x,y) = \mu\frac{2N}{\pi a^3 b}\left(x_l^2(y) - x^2\right) \tag{18}$$

where N is the normal force and μ is the friction coefficient.

5 Results of FASTSIM for a SDEC region and comparison with other FASTSIM versions

Three versions of the FASTSIM algorithm for non-Hertzian contacts are compared in this section, and the CONTACT program is used as the reference to assess the performance of these simplified models.

The FASTSIM versions considered are:

- the extension of FASTSIM for SDEC regions proposed in this paper, denoted as FASTSIM-SDEC;
- the standard FASTSIM for non-elliptic contact with the three flexibility parameters determined from an equivalent ellipse as described in reference [16]. This method is denoted FASTSIM-EQ.L. This version takes the real non-elliptic contact area into account in the calculation of the stresses and resultant forces as FASTSIM-SDEC, but the flexibility parameters are determined without considering the actual non-elliptic shape;
- the equivalent ellipse method: the original FASTSIM algorithm for elliptic contacts is applied to an equivalent ellipse approximating the non-elliptic patch, see [36]. This method is denoted FASTSIM-EQ.E which is essentially a Hertzian model.

To ensure the exact matching of the contact patch geometry with the two versions of FASTSIM considering a non-elliptic contact patch, the reference solution is computed using CONTACT-SDEC.

It should be noted that in method FASTSIM-EQ.E the equivalent ellipse is usually introduced by taking the origin at the same location as that of the actual non-elliptic contact area, as shown by the red dashed line in Figure 4. However, this choice may lead to an inaccurate evaluation of the total creep force, because the effect of spin on the longitudinal creep force is missed. A significant error arising from this choice is also introduced in the evaluation of quantities related to wheel wear such as the $T\gamma$ product [37], due to the mismatch between the equivalent contact area and the actual contact area in lateral direction which causes inaccurate prediction of the location of wear on the wheel profile, see the results presented in [38].

A shifting of the centre of the equivalent ellipse can be used to obtain a better matching of the equivalent ellipse to the actual non-elliptic shape of the contact patch. This requires that the centre of the equivalent ellipse is shifted by y_0 in lateral direction, as shown by the blue dashed line in Figure 4. This correction is expected to improve the accuracy of the FASTSIM-EQ.E solution in terms of the total force and wear over a non-elliptic contact patch. Considering that the creepages determined from the kinematics of MBS simulation are defined at the same position on the wheel, often the initial contact point, no matter what type of local contact model is used, the longitudinal creepage ν_x shall be corrected in the same way as done for CONTACT-SDEC, see Eq.(10). In addition, if this contact model is used in an MBS simulation, the change in the point of application of the total forces and moment caused by the change of the contact origin from *O* to *O'* shall be taken into account. Reference [27] provides a comprehensive discussion of the implications of the choice of the reference point in the contact region at which the creepages are defined.

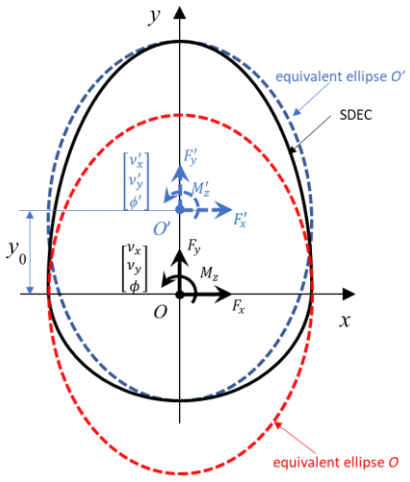

Figure 4 Approximation of the SDEC contact region as an equivalent ellipse in FASTSIM-EQ.E method.

A series of contact cases are considered to assess the performance of the three FASTSIM formulations, all sharing the following common inputs: a = 4.25 mm, shear modulus G = 80 GPa, Poisson's ratio υ = 0.25, and friction coefficient μ = 0.35. The results are compared in the following two sub-sections in terms of the total contact force components.

Figure 5 compares the normalised longitudinal and lateral forces F_x and F_y for ellipticity g = 1.0, shape number ψ = 0.6 under pure spin condition, i.e. zero longitudinal and lateral creepages at the initial contact point, for different values of spin in the range of 0 ÷ 1.6 m^{-1}. The deviations between the three versions of FASTSIM and CONTACT are reported in the same figure on the right. It should be noted that for the FASTSIM-EQ.E, a corrected longitudinal creep defined by Eq. (10) is used. This means that a pure spin condition ($\nu_x = \nu_y = 0$ and $\phi \neq 0$) defined at point O in Figure 4 for the other models leads to a non-zero value of the corrected longitudinal creepage ($\nu_x' = \nu_x - \phi y_0 \neq 0$) at point O' for the FASTSIM-EQ.E. Hereafter, the term "pure spin condition" is used to denote a case in which the longitudinal and lateral creepages are both zero at the initial contact point O.

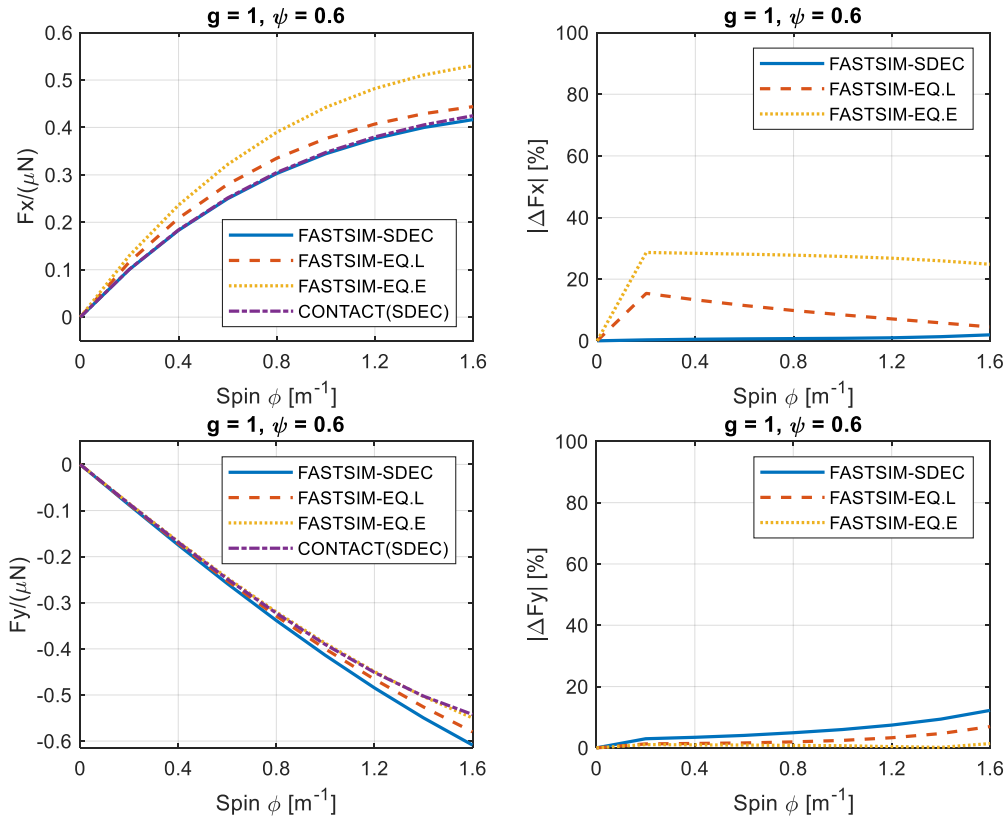

Figure 5 Ellipticity and asymmetry held fixed (g = 1.0, ψ = 0.6), spin varying: normalised creep forces vs. spin creepage and deviations from the reference solution given by CONTACT

The proposed method FASTSIM-SDEC shows very good agreement to the reference longitudinal creep force from CONTACT with a maximum deviation below 2% while the deviation observed for the FASTSIM-EQ.L method and the FASTSIM-EQ.E method are around 10% and 30%, respectively. As far as the lateral force is concerned, the differences among the three FASTSIM implementations are below 5% except for large spin values. The deviation between FASTSIM-SDEC and FASTSIM-EQ.L is exclusively due to the way in which the flexibility parameters are determined, whereas the deviations between FASTSIM-EQ.E and the other methods are due to multiple causes apart from the determination of the flexibility parameters, namely a different distribution of the slip in the contact region, the fact that FASTSIM-EQ.E considers an elliptic approximation of the domain over which the contact stresses are integrated to produce the resulting creep forces and the fact that the distribution of the traction bound in the equivalent ellipse used by FASTSIM-EQ.E differs from the distribution of the traction bound in the SDEC region.

Figure 6 compares the results of the three FASTSIM implementations in terms of the normalised creep forces F_x and F_y as a function of the shape number for a pure spin condition with ϕ = 1.0 m^{-1}(v_x = v_y = 0) and for ellipticity g = 1.0 (same value as in the previous test case). The deviations from the reference solution provided by CONTACT are shown in the same figure in the right column. These results show that the longitudinal force under pure spin condition is linearly increasing with the shape number, an observation consistent with the linear theory for the SDEC region, where the new coefficient C_{13}^{s} is a linear function of the shape number. The proposed FASTSIM-SDEC algorithm shows good agreement to the reference in terms the longitudinal creep force, with a maximum deviation from CONTACT below 2%, whilst for FASTSIM-EQ.L and FASTSIM-EQ.E the deviation is approximately 10% and 30%, respectively, in a large range of values of the shape number. As far as the

lateral component of the creep force is concerned, all the three versions of FASTSIM provide an accurate approximation of the solution from CONTACT, with deviations generally in the range of 5% or lower and the differences between the three approaches are not so much worth of notice.

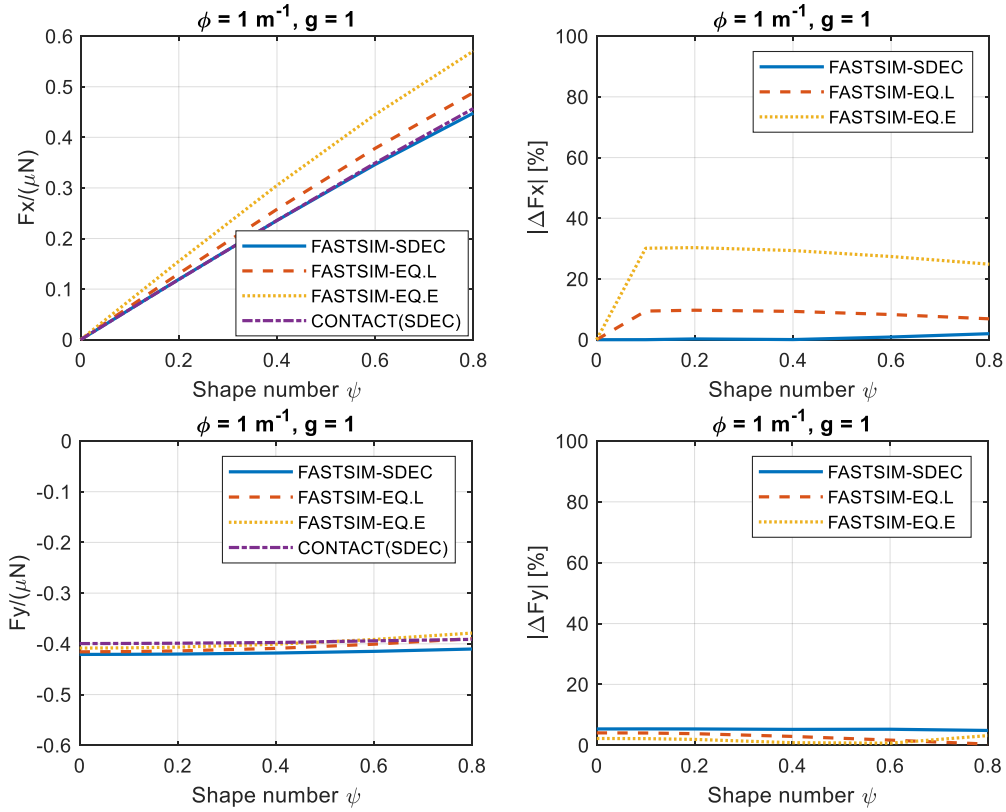

Figure 6 Ellipticity and spin held fixed (g = 1.0, ϕ = 1 m^{-1}), asymmetry varying: normalised creep forces as a function of the shape number and deviations from the reference solution given by CONTACT

Figure 7 shows the normalised longitudinal force F_x and lateral force F_y from different implementations of the FASTSIM algorithm as a function of the ellipticity g for a pure spin creepage ϕ = 1.0 m^{-1} ($v_x = v_y = 0$ in the initial contact point) considering a fixed value of the shape number ψ = 0.6 (same value as in the first test case). The deviations from the reference solutions given by CONTACT are reported in the same figure in the right column. These results show that the longitudinal component of the creep force from the FASTSIM-SDEC algorithm is once more in excellent agreement with the reference for all the ellipticity values considered, whilst significantly larger deviations are observed for both the FASTSIM-EQ.L and FASTSIM-EQ.E versions of the algorithm. The trend with ellipticity g of the relative deviations between the three FASTSIM versions and the reference solution may become misleading at large values of g, because the longitudinal force approaches zero and therefore small deviations in terms of the absolute value of the force lead to large relative deviations. Like in the other cases considered previously, the lateral forces obtained from different versions of FASTSIM are generally in good agreement with each other and with the reference solution, except for small values of ellipticity $g < 0.2$ where large deviations from the reference solution, up to 100% and more, are observed for all FASTSIM versions. This may be due to the assumption of a linear distribution of shear stresses in the adhesion area which is inherent to the simplified theory but may lead to significant inaccuracy if applied in a contact patch which is very slender in the lateral direction.

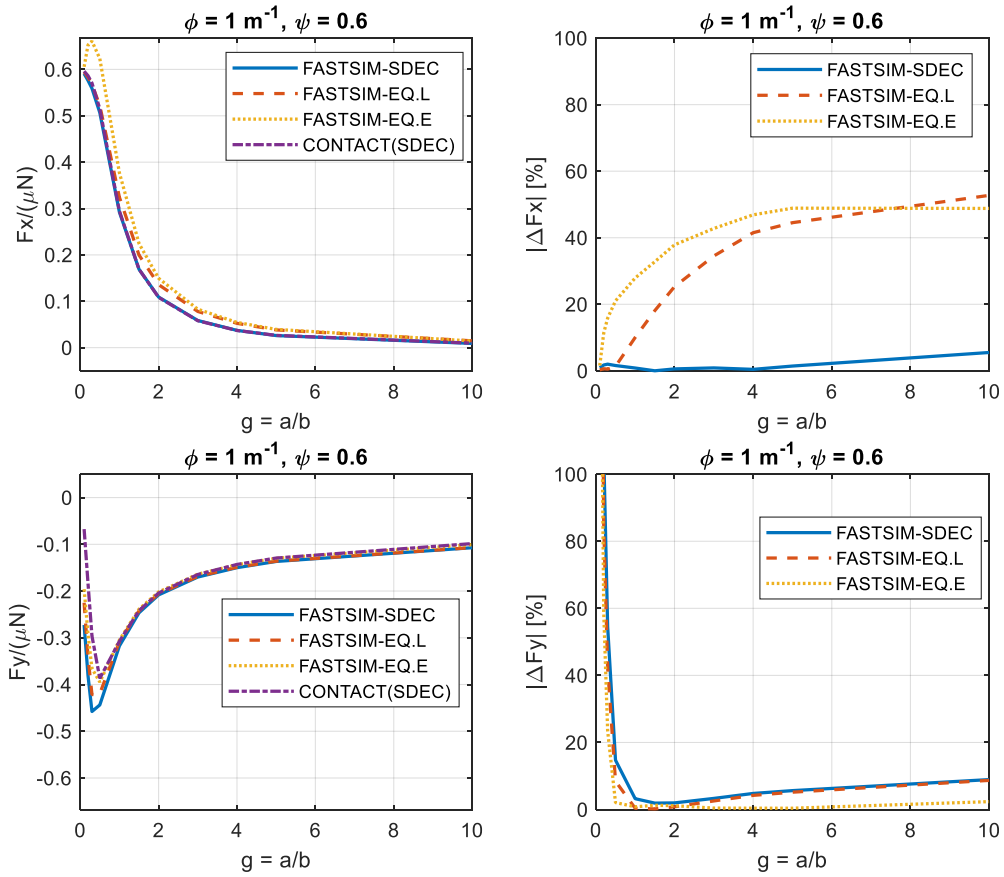

Figure 7 Asymmetry and spin held fixed (ψ = 0.6, ϕ = 1 m^{-1}), ellipticity varying: normalised creep forces as a function of the ellipticity and deviations from the reference solution given by CONTACT

To summarize, the FASTSIM algorithm for a SDEC region proposed in this paper provides satisfactory accuracy in the determination of the total creep force for a wide variety of SDEC patches (except pure spin conditions at very low values of eccentricity), and a more accurate prediction of the longitudinal creep force compared to the other two FASTSIM implementations considered in this study. Since the FASTSIM algorithm is not only able to compute the total creep force components but also provides as an output the distribution of stresses and $T\gamma$ wear number over the contact patch, it can be expected that the proposed method can be also improve the accuracy of wheel profile wear prediction, which is the topic of an ongoing research project.

Conclusions

A generalisation of Kalker's classic linear theory of rolling contact to non-elliptic contact patches that can be approximated as a SDEC region is proposed. In this extended linear theory, the coefficients of the original linear theory for elliptic patches are maintained and four new coefficients are introduced to consider the effect of non-ellipticity. The additional computational complexity involved with applying the generalised linear theory for a SDEC region instead of the 'classic' linear theory for elliptic patches is very limited, therefore the new theory can be easily applied to a number of cases where non-Hertzian contact patches are formed between wheels and rails.

The generalised linear theory can also be used to extend to non-elliptic contact patches any existing non-linear creep force model making use of the linear theory, such as heuristic saturation laws like Shen-Hedrick-Elkins. To demonstrate this idea, an extension of the

FASTSIM algorithm for a SDEC region is developed in this paper and compared with existing implementations of FASTSIM, using results from CONTACT as a term of reference. Numerical experimental results show that the FASTSIM algorithm for a SDEC region developed in this paper provides satisfactory accuracy in the determination of the total creep force for a wide variety of SDEC patches, with the exception pure spin conditions for contact patches having very low ellipticity values, i.e. $g < 0.2$, for which significant deviations from CONTACT are observed for all FASTSIM implementations considered, including the new one developed in this paper. It is also observed that the new FASTSIM implementation is significantly more accurate than other existing versions of the algorithm in predicting the longitudinal creep force for pure spin conditions.

The results presented in this paper focus exclusively on spin influence for SDEC-type regions, therefore, one direction of future work in this project is to consider the effect of non-ellipticity of the contact patch in cases when a mix of longitudinal/lateral/spin creepages is considered. Another future development foreseen is to incorporate the newly developed version of FASTSIM in MBS models for rail vehicle dynamics simulation, to investigate the influence of non-Hertzian contact conditions on the results of MBS simulations. The third direction for further research is to assess the accuracy of FASTSIM for SDEC regions as a fast but hopefully accurate method for the prediction of wheel wear.

References

[1] P. Oldrich, B. Mats, and S. Iwnick, "Simulation of Railway Vehicle Dynamics," in *Handbook of railway vehicle dynamics*, 2nd ed., S. Iwnicki, M. Spiryagin, C. Cole, and T. McSweeney, Eds. London: CRC Press LLC, 2020, pp. 651–722.

[2] F. Braghin, S. Bruni, and R. Lewis, "Railway wheel wear," in *Wheel-rail interface handbook*, R. Lewis and U. Olofsson, Eds. Oxford: Woodhead Publishing Limited, 2009, pp. 172–206.

[3] A. Ekberg, "Fatigue of railway wheels," in *Wheel-rail interface handbook*, R. Lewis and U. Olofsson, Eds. Oxford: Woodhead Publishing Limited, 2009, pp. 211–242.

[4] J. J. Kalker, *Three dimensional elastic bodies in rolling contact*. Dordrecht/Boston/London: Kluwer Academic Publishers, 1990.

[5] J. Ayasse, H. Chollet, and M. Sebès, "Wheel-Rail Contact Mechanics," in *Handbook of Railway Vehicle Dynamics*, 2nd ed., S. Iwnicki, M. Spiryagin, C. Cole, and T. McSweeney, Eds. London: CRC Press LLC, 2020, pp. 242–278.

[6] S. Z. Meymand, A. Keylin, and M. Ahmadian, "A survey of wheel–rail contact models for rail vehicles," *Veh. Syst. Dyn.*, vol. 54, no. 3, pp. 386–428, 2016.

[7] B. Liu and S. Bruni, "Comparison of wheel–rail contact models in the context of multibody system simulation: Hertzian versus non-Hertzian," *Veh. Syst. Dyn.*, 2020.

[8] E. Vollebregt, K. Six, and O. Polach, "Challenges and progress in the understanding and modelling of the wheel–rail creep forces," *Veh. Syst. Dyn.*, vol. 59, no. 7, pp. 1026–1068, 2021.

[9] S. Beretta, F. Braghin, G. Bucca, and H. Desimone, "Structural integrity analysis of a tram-way: Load spectra and material damage," *Wear*, vol. 258, no. 7–8, pp. 1255–1264, 2005.

[10] A. Ekberg, E. Kabo, J. C. O. Nielsen, and R. Lundén, "Subsurface initiated rolling contact fatigue of railway wheels as generated by rail corrugation," *Int. J. Solids Struct.*, vol. 44, no. 24, pp. 7975–7987, 2007.

[11] T. Jendel, “Prediction of wheel profile wear-comparisons with field measurements,” *Wear*, vol. 253, pp. 89–99, 2002.

[12] B. Liu, S. Bruni, and R. Lewis, “Numerical calculation of wear in rolling contact based on the Archard equation: Effect of contact parameters and consideration of uncertainties,” *Wear*, vol. 490–491, no. November 2021, p. 204188, 2021.

[13] R. Enblom and M. Berg, “Impact of non-elliptic contact modelling in wheel wear simulation,” *Wear*, vol. 265, no. 9–10, pp. 1532–1541, 2008.

[14] G. Tao, Z. Wen, X. Zhao, and X. Jin, “Effects of wheel–rail contact modelling on wheel wear simulation,” *Wear*, vol. 366–367, pp. 146–156, 2016.

[15] E. A. H. Vollebregt, “User guide for CONTACT v21.1: Rolling and sliding contact with friction,” Rotterdam, The Netherlands, 2021.

[16] J. Piotrowski and W. Kik, “A simplified model of wheel/rail contact mechanics for non-Hertzian problems and its application in rail vehicle dynamic simulations,” *Veh. Syst. Dyn.*, vol. 46, no. 1–2, pp. 27–48, 2008.

[17] B. Liu, S. Bruni, and E. Vollebregt, “A non-Hertzian method for solving wheel–rail normal contact problem taking into account the effect of yaw,” *Veh. Syst. Dyn.*, vol. 54, no. 9, pp. 1226–1246, 2016.

[18] M. Sh. Sichani, R. Enblom, and M. Berg, “A novel method to model wheel–rail normal contact in vehicle dynamics simulation,” *Veh. Syst. Dyn.*, vol. 52, no. 12, pp. 1752–1764, 2014.

[19] J. Ayasse and H. Chollet, “Determination of the wheel rail contact patch in semi-Hertzian conditions,” *Veh. Syst. Dyn.*, vol. 43, no. 3, pp. 161–172, 2005.

[20] J. P. Pascal and G. Sauvage, “Vehicle System Dynamics : International Journal of Vehicle Mechanics and Mobility The Available Methods to Calculate the Wheel / Rail Forces in Non Hertzian Contact Patches and Rail Damaging,” vol. 22, pp. 263–275, 1993.

[21] S. Bruni, R. Goodall, T. X. Mei, and H. Tsunashima, “Control and monitoring for railway vehicle dynamics,” *Veh. Syst. Dyn.*, vol. 45, no. 7–8, pp. 743–779, 2007.

[22] A. De Rosa, S. Alfi, and S. Bruni, “Estimation of lateral and cross alignment in a railway track based on vehicle dynamics measurements,” *Mech. Syst. Signal Process.*, vol. 116, pp. 606–623, 2019.

[23] J. Evans and M. Berg, “Challenges in simulation of rail vehicle dynamics,” *Veh. Syst. Dyn.*, vol. 47, no. 8, pp. 1023–1048, 2009.

[24] J. J. Kalker, “A Fast Algorithm for the Simplified Theory of Rolling Contact,” *Veh. Syst. Dyn.*, vol. 11, no. 1, pp. 1–13, 1982.

[25] J. Piotrowski, B. Liu, and S. Bruni, “The Kalker book of tables for non-Hertzian contact of wheel and rail,” *Veh. Syst. Dyn.*, vol. 55, no. 6, pp. 875–901, 2017.

[26] J. Piotrowski, S. Bruni, E. Di Gialleonardo, and B. Liu, “A fast method for determination of creep forces in non-Hertzian contact of wheel and rail based on a book of tables,” *Multibody Syst Dyn*, vol. 45, pp. 169–184, 2019.

[27] E. A. H. Vollebregt, “Comments on ‘the Kalker book of tables for non-Hertzian contact of wheel and rail,’” *Veh. Syst. Dyn.*, vol. 56, no. 9, pp. 1451–1459, 2018.

[28] A. Alonso and J. G. Giménez, “Tangential problem solution for non- elliptical contact areas with the FastSim algorithm,” *Veh. Syst. Dyn.*, vol. 45, no. 4, pp. 341–357, 2007.

[29] E. A. H. Vollebregt, “Survey of programs on contact mechanics developed by J.J.

Kalker," *Veh. Syst. Dyn.*, vol. 46, no. 1–2, pp. 85–92, 2008.

[30] S. Fukagai, T. Toyama, T. Tanaka, M. Kuzuta, and H. Doi, "Visualization of wheel-rail contact area of running vehicle using film sensor," *Proc. Inst. Mech. Eng. Part F J. Rail Rapid Transit*, 2021.

[31] R. S. Dwyer-Joyce, C. Yao, J. Zhang, R. Lewis, and B. W. Drinkwater, "Feasibility study for real time measurement of wheel-rail contact using an ultrasonic array," *J. Tribol.*, vol. 131, no. 4, pp. 1–9, 2009.

[32] K. L. Johnson, *Contact Mechanics*. Cambridge, UK: Cambridge University Press, 1985.

[33] Z. Y. Shen, J. K. Hedrick, and J. A. Elkins, "A Comparison of Alternative Creep Force Models for Rail Vehicle Dynamic Analysis," *Veh. Syst. Dyn.*, vol. 12, no. 1–3, pp. 79–83, 1983.

[34] E. A. H. Vollebregt and P. Wilders, "FASTSIM2: A second-order accurate frictional rolling contact algorithm," *Comput. Mech.*, vol. 47, no. 1, pp. 105–116, 2011.

[35] M. Sh. Sichani, R. Enblom, and M. Berg, "An alternative to FASTSIM for tangential solution of the wheel–rail contact," *Veh. Syst. Dyn.*, vol. 54, no. 6, pp. 748–764, 2016.

[36] E. A. H. Vollebregt, C. Weidemann, and A. Kienberger, "Use of 'CONTACT' in Multi-Body Vehicle Dynamics and Profile Wear Simulation: Initial Results," *22nd Int. Symp. Dyn. Veh. Roads Tracks*, pp. 1–6, 2011.

[37] T. G. Pearce and N. D. Sherratt, "Prediction of wheel profile wear," *Wear*, vol. 144, no. 1–2, pp. 343–351, 1991.

[38] M. Sh. Sichani, R. Enblom, and M. Berg, "A fast wheel–rail contact model for application to damage analysis in vehicle dynamics simulation," *Wear*, vol. 366–367, pp. 123–130, 2016.